

Experimental Demonstration of a Multi-Beam Antenna with Full Parameters Based on Inductor-Capacitor Networks

Chengfu Yang¹, Ming Huang^{1, *}, Haozheng Zhang¹, Jingjing Yang¹,
Tinghua Li², Peng Li¹, and Fuchun Mao³

Abstract—In this paper, we experimentally demonstrate the performance of a multi-beam antenna based on inductor-capacitor (L-C) transmission line networks. The lumped element parameters of the antenna are derived according to the mapping relations between Maxwell's equations and L-C network equations. The simulation results are in good agreement with the measurement ones, and the antenna performs well at a wide bandwidth with high directivity. The antenna has potential applications in future communication systems.

1. INTRODUCTION

Transformation optics (TO) [1–3], which is based on the form invariance of Maxwell's equations, has attracted significant attention in the design of novel electromagnetic and optical devices to guide waves along predesigned routes. Many novel devices based on TO theory have been proposed and implemented, including cloaks [4–8], concentrators [9–11], illusion devices [12–14], and lens [15–18]. Among these devices, multi-beam antennas capable of achieving multi-beam emission show promise for many potential applications in the fields of satellite communications, smart traffic systems, and multiple-input multiple-output (MIMO) systems [19–24]. However, the spatially inhomogeneous and highly anisotropic material parameters of the early transformation-based multi-beam antennas represent a considerable challenge for fabrication [19, 22]. In an effort to develop devices for practical application, multi-beam antennas with fewer material parameters have been proposed and implemented, such as antennas consisting of anisotropic zero-index materials [20] and uniaxial zero-index materials [21, 23]. Although these antennas have fewer material parameters than earlier antennas, the inherent resonance characteristics of the split-ring resonators and inductor-capacitor (LC) resonators used in the antennas result in a narrow bandwidth and relatively poor performance of the device. Recently, a novel multi-beam antenna consisting of non-zero index, block homogeneous and isotropic materials was proposed based on a piecewise conformal TO (PCTO) approach [24], which is relatively easy to implemented. The PCTO approach is attractive, but to the best of our knowledge, it is still in the theoretical research stage.

In this paper, a four-beam antenna based on the PCTO method is experimentally demonstrated by utilizing periodic L-C transmission line networks. The lumped element parameters of the antenna are derived, and numerical simulations are performed. A prototype of the antenna with all the parameters is fabricated, and the antenna performance is evaluated. The simulated and experimental results of the near-field distribution and far-field pattern of the designed antenna are in excellent agreement, verifying the accuracy and validity of the experiment. Wide bandwidth and high directivity are observed in the simulation and experiment.

Received 23 March 2020, Accepted 4 June 2020, Scheduled 14 June 2020

* Corresponding author: Ming Huang (huangming@ynu.edu.cn).

¹ School of Information Science and Engineering, Yunnan University, Kunming, Yunnan 650091, China. ² Technical Center of China Tobacco Yunnan Industrial Co. Ltd., Kunming, Yunnan 650231, China. ³ Institute of Criminal Investigation, Yunnan Police College, Kunming, Yunnan 650223, China.

2. METHOD AND MODEL

Figure 1 shows the scheme of the transformation procedure of the PCTO method [24]. The circle in the virtual space is transformed into a square in the physical space. Both the virtual space and physical space are divided into N subregions by partitioning the angle from 0 to 2π around O and O' into N angles θ_i , $i = 1, 2, \dots, N$ and $\sum_{i=1}^N \theta_i = 2\pi$. The radii of the sector A_iOA_{i+1} with the center angle θ_i in the virtual space are defined as $R_i = R = (|OA_i| + |OA_{i+1}|)/2$, where R is the radius of the circle. In the physical space, the subregion $A'_iOA'_{i+1}$ is approximated by a sector $B'_iOB'_{i+1}$ with the same center angle θ_i ; the radii of the sector $B'_iOB'_{i+1}$ are defined as $R'_i = (|OA'_i| + |OA'_{i+1}|)/2 = (|OB'_i| + |OB'_{i+1}|)/2$, as shown in Fig. 1(c). The sectors A_iOA_{i+1} and $B'_iOB'_{i+1}$ are similar to each other, and the transformation between the virtual space and physical space is conformal. As a result, only the ε_z component is variable and is determined by the transformation function of the Jacobian matrix in a transverse electric (TE) mode. The material parameters of the transformation medium are expressed as [24]:

$$\varepsilon_z = \frac{\varepsilon}{|J|} = \varepsilon \left(\frac{R_i}{R'_i} \right)^2, \quad \mu = 1. \quad (1)$$

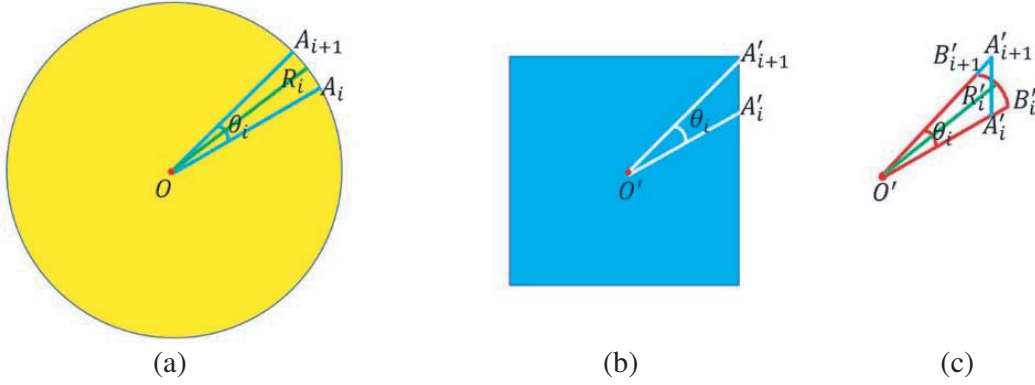


Figure 1. Scheme of the PCTO method. (a) The virtual space. (b) The physical space. (c) i th subregion in the physical space approximated by a sector with the radius R'_i .

According to electromagnetic theory and transmission line theory, a mapping relationship exists between the L-C network equations and the polarized TE (transverse electric) or transverse magnetic (TM) Maxwell equations; the voltages V and currents I are mapped to the field quantities E and H respectively. In the case of a long-wavelength limit, the dimension of the unit cell Δ is much smaller than the wavelength of the excitation source, and the two-dimensional (2D) L-C transmission line network can be used to mimic a 2D isotropic medium whose material parameters are governed by Eq. (1). In the TE mode, the relationship between the material parameters and L-C transmission line network can be expressed as [12, 25–27]:

$$\begin{cases} \mu_x = \mu\mu_0 = L_x/\Delta, \\ \mu_y = \mu\mu_0 = L_y/\Delta, \\ \varepsilon_z = \varepsilon_z\varepsilon_0 = C_z/\Delta. \end{cases} \quad (2)$$

where Δ is the dimension of the unit cell; L_x and L_y are the series inductances in the x - and y -directions; C_z is the shunt capacitance in the z -direction of the unit cell; μ_0 and ε_0 are the permeability and permittivity of the free space, respectively; μ_x and μ_y are the permeability in the x - and y -directions; and ε_z is the permittivity in the z -direction, i.e., the polarized direction of the electric field in the TE mode. The left parts of Eq. (2) represent the material constitutive parameters, and the right parts denote the value and dimension of the lumped parameter components.

The dimension of the unit cell is $\Delta = 6$ mm in this work to meet the limit of the long-wavelength condition; this value is much smaller than the wavelength of the excitation source ($f_0 = 50$ MHz). For the sake of the measurements, we fabricate a sample of the L-C network with lumped reactive elements

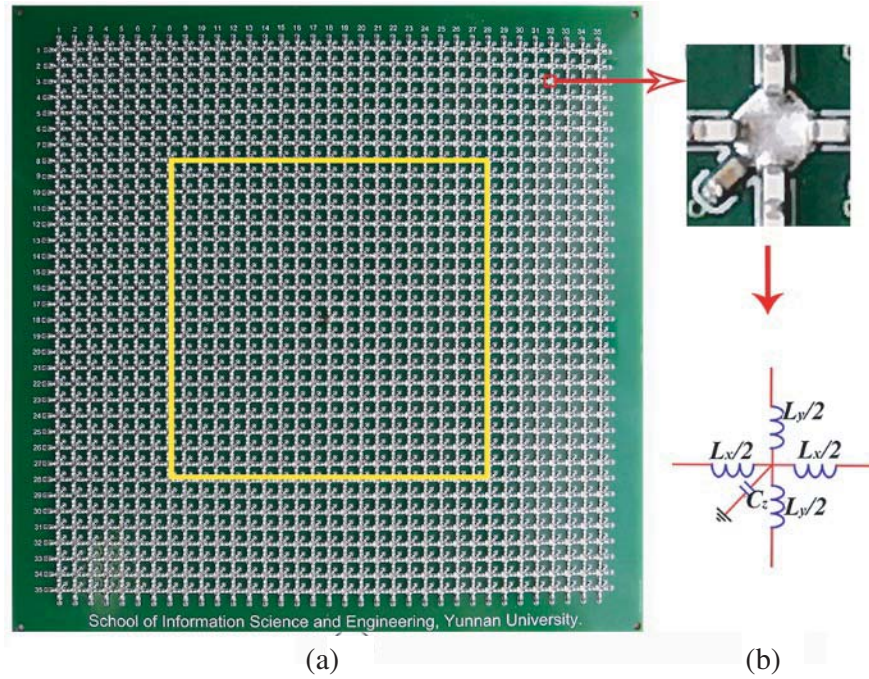


Figure 2. Photograph of the sample of the four-beam antenna and the unit cell of the L-C network.

on an FR-4 substrate with a dielectric constant of 4.3 and thickness of 1 mm, as shown in Fig. 2(a), where the yellow-colored lines denote the boundaries of the four-beam antenna. Each unit of the L-C component (including the background and transformation medium) consists of four surface-mounted inductors in series and one capacitor shunted to the ground by a via-hole, as shown in Fig. 2(b). A package size of 0603 of the surface-mounted inductors and capacitors is used to mimic the transformation medium and background.

The physical space consists of a square area with a side length of 21Δ , and the virtual space consists of a circular area that is the circum circle of the square. A segmentation angle of $\theta_i = 10^\circ$ is chosen, and the permittivity distribution of the transformation medium is calculated using the COMSOL Multiphysics software, as shown in Fig. 3(a). The background medium is $n = \sqrt{\epsilon_b \mu_b} = 100$ with

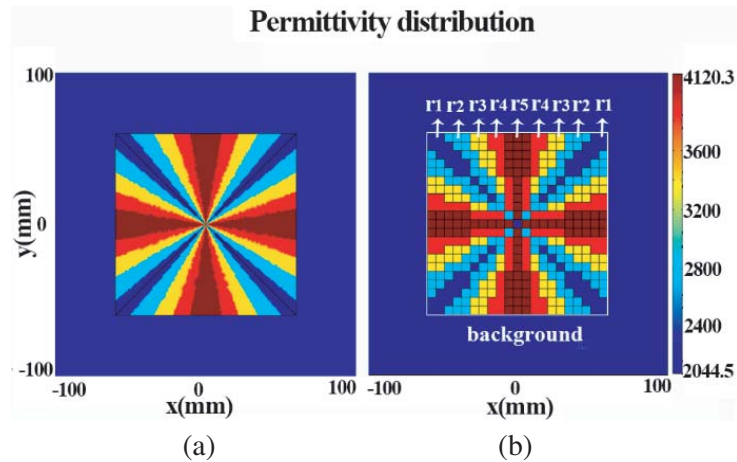


Figure 3. The permittivity distribution of the four-beam antenna; the background has a medium of $\epsilon_b = 2094$ and $\mu_b = 4.78$ and a segmentation angle of $\theta_i = 10^\circ$. (a) The continuous distribution of the permittivity and (b) the discretized distribution of the permittivity.

Table 1. The parameters of the simulation and experiments of the four-beam antenna.

Regions		Background	r1	r2	r3	r4	r5
COMSOL	ε_z	2092	2044.5	2765.4	3399.3	3869.9	4120.3
	$\mu_x = \mu_y$	4.78	4.78	4.78	4.78	4.78	4.78
Theoretical values (ADS)	C_z (pF)	111	108.6	146.9	180.6	205.6	218.9
	$L_x = L_y$ (nH)	36	36	36	36	36	36
Available values (ADS and sample)	C_z (pF)	110	110	150	180	200	220
	$L_x = L_y$ (nH)	36	36	36	36	36	36

$\mu_b = 4.78\mu_0$, $\varepsilon_b = 2092\varepsilon_0$ in our simulation, and the inductance and capacitance values of this medium are $L_x = L_y = 36$ nH and $C_z = 111$ pF, respectively. The sample has a dimension of $250 \text{ mm} \times 250 \text{ mm}$. It is observed that the transformation medium consists of 5 types of dielectrics whose permittivity values range from 2044.5 to 4120.3. Fig. 3(b) shows the discretization result of Fig. 3(a), where the symbols $r1$ – $r5$ represent the five regions that are filled with different materials. Due to symmetry and for brevity, the denotations are omitted in the quarter block on the left, right, and lower sides of the transformation medium. Table 1 lists the permittivity and permeability values of the proposed antenna, as well as the equivalent inductance and capacitor values used in the simulations and experiments. Rows 2 and 3 list the values used in the COMSOL simulation; rows 4 and 5 are the values used for the theoretical simulation in the Agilent advanced design system (ADS); and rows 6 and 7 are the values used in the ADS simulation and the experiment. During the ADS simulation and sample measurement, Bloch impedances with a resistance of about 18Ω are used to truncate the outer boundary of the device. The sample consists of 35×35 grid nodes.

3. RESULTS AND DISCUSSION

Figures 4(a) and 4(e) show the field distributions of the designed four-beam antenna obtained from the COMSOL Multiphysics software; cylindrical waves were excited at the origin of the device with operating frequency of 50 MHz and 75 MHz. The cylindrical wave is split into four beams successfully when the electromagnetic field passes through the device. Figures 4(b), 4(c), 4(f), and 4(g) depict the voltage distributions of the antenna obtained from the ADS simulation when a point source (with a frequency of 50 MHz (upper row) and 75 MHz (bottom row)) is excited at the origin located at the grid node (18, 18). Figs. 4(b) and 4(f) show the simulation results when the theoretical values listed in lines 4 and 5 of Table 1 while Figs. 4(c) and 4(g) show the simulation results when the available values are used (rows 6 and 7 in Table 1). The current source is split into four beams successfully, which is in excellent agreement with the result from the COMSOL simulation. In addition, it is observed that although the available components are slightly different from the theoretical components, the near-field voltage distributions are almost identical.

We fabricated the antenna sample shown in Fig. 2(a) and confirmed the simulation results using an experiment. The sample consisted of 35×35 grid nodes, i.e., 35 grid nodes in the x -direction and 35 grid nodes in the y -direction. The Agilent network analyzer PNA3783 was used to measure the sample. One port of the PNA3783 was connected to node (18, 18) through a coaxial-cable welded on the back of the circuit board to provide a time-harmonic signal, and the other port of PNA3783 was connected to a high-impedance probe to obtain the transmission coefficients of the nodes. The voltage distribution was determined based on the transmission coefficient. We measured the sample at 50 MHz and 75 MHz and plotted the voltage distribution using the raw data, as shown in Figs. 4(d) and 4(h). The simulation results are in agreement with the experimental data. The electromagnetic waves interact with the transformation medium, and the original propagation pattern is split into four beams that travel through the medium. As shown in Figs. 4(e)–4(h), although the operating frequency (75 MHz) in the experiment is much higher than the designed operating frequency ($f_0 = 50$ MHz), the device still performs well, indicating that it can perform well at a wide bandwidth. This result is attributed to the non-resonance nature of the PCTO method.

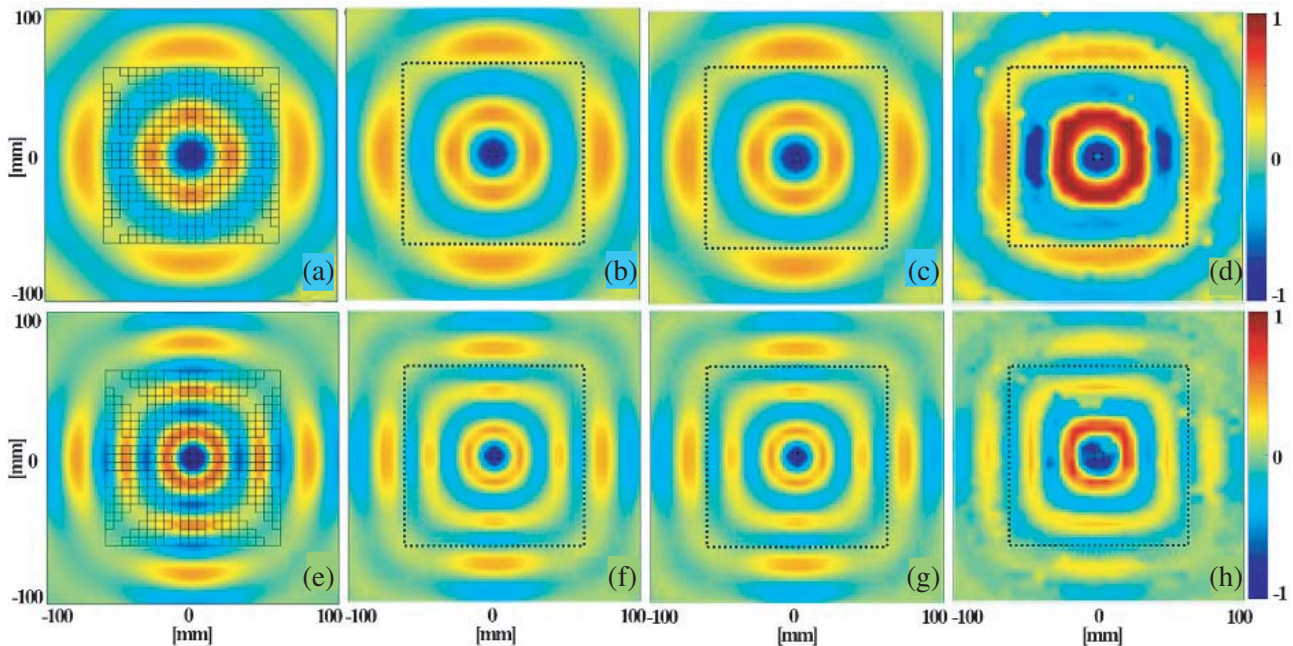


Figure 4. Electromagnetic field distribution obtained from the COMSOL simulation at (a) 50 MHz and (e) 75 MHz. Voltage distribution snapshot obtained from the ADS simulation at (b) 50 MHz and (f) 75 MHz using theoretical values and at (c) 50 MHz and (g) 75 MHz using available components. Experimental voltage distribution snapshots obtained at (d) 50 MHz and (h) 75 MHz using available components. The dashed black lines denote the outer boundaries of the designed antenna.

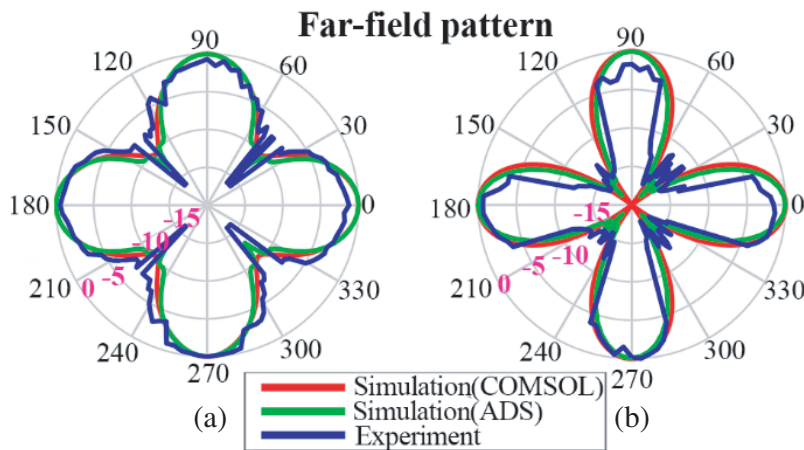


Figure 5. Far-field patterns of the designed antenna obtained from the COMSOL simulation (red curve), ADS simulation (green curve), and the experiment (blue curve). The operating frequencies are (a) 50 MHz and (b) 75 MHz.

The directivity of the designed four-beam antenna is investigated; the far-field patterns of the device obtained from the simulation experiment are shown in Fig. 5. It should be noted that the measured far-field pattern of the antenna is approximated using the second norm difference of the voltage ($(|V|/|V|_{\max})^2$) at the outermost nodes of the sample, where $|V|_{\max}$ is the maximum value of the voltage norm and is equal to the voltage amplitude of the center node (18, 18). At $f = 50$ MHz, the directivity of the antenna is 11.2 dB (using the available values) for both the simulation results from COMSOL and ADS, whereas the experimental result of the sample is about 7.5 dB, as shown in

Fig. 5(a). However, at $f = 75$ MHz, the antenna directivity is 23 dB for COMSOL, 16 dB for ADS, and 11.8 dB for the experiment, as shown in Fig. 5(b). The slight differences between the simulated and experimental results might have been caused by the comparatively large tolerance (about 10%) of the inductor and capacitor elements, the loss due to the dielectric substrate, and measurement errors. The performance of the sample would be higher if these factors could be controlled. Nonetheless, both the simulated and experimental results demonstrate that the antenna designed by the PCTO method exhibits excellent directivity and bandwidth and might be well suited for satellite communications, smart traffic systems, and MIMO systems. It should be noted that the L-C network approach based on lumped parameter components is only effective in low-frequency band, and the unit size should be much smaller than the operating wavelength ($\lambda/20$). In this case, the parasitic effect of the lumped component is negligible. However, at high frequencies, e.g., satellite communications and smart traffic systems, a distributed parameter circuit model, such as a microstrip line and interdigitated capacitance, can be used in the antenna. Furthermore, Eq. (1) indicates that the relative permittivity of the antenna can exceed 1 by carefully tuning the dimensions of the virtual space and physical space, and drilling holes on the dielectric substrate can be used to achieve the proposed antenna.

4. CONCLUSIONS

In summary, a PCTO-based four-beam antenna was designed and fabricated. The antenna operation was based on L-C transmission line networks. The numerical simulation and experimental results demonstrated that the antenna performed well for beam splitting and operated at a wide bandwidth with high directivity. It is believed that the proposed method provides a valuable reference for accelerating the practical application of the PCTO-based four-beam antennas; the method can also be applied to other PCTO-based devices.

ACKNOWLEDGMENT

This work was funded by the National Natural Science Foundation of China (Grant Nos. 61461052, 11564044, 61863035), and was supported by the Key Program of Natural Science of Yunnan Province (Grant Nos. 2013FA006, 2015FA015).

REFERENCES

1. Pendry, J. B., D. Schurig, and D. R. Smith, "Controlling electromagnetic fields," *Science*, Vol. 312, No. 5781, 1780–1782, 2006.
2. Leonhardt, U., "Optical conformal mapping," *Science*, Vol. 312, No. 5781, 1777–1780, 2006.
3. Jiang, W. X., W. X. Tang, and T. J. Cui, "Transformation optics and applications in microwave frequencies," *Progress In Electromagnetics Research*, Vol. 149, 251–273, 2014.
4. Schurig, D., J. J. Mock, B. J. Justice, S. A. Cummer, J. B. Pendry, A. F. Starr, and D. R. Smith, "Metamaterial electromagnetic cloak at microwave frequencies," *Science*, Vol. 314, No. 5801, 977–980, 2006.
5. Li, J. and J. B. Pendry, "Hiding under the carpet: A new strategy for cloaking," *Physical Review Letters*, Vol. 101, No. 20, 203901, 2008.
6. Yang, Y. H., S. S. Lin, Z. J. Wang, H. Chen, H. Wang, and E. Li, "Three-dimensional polyhedral invisible cloak consisting of homogeneous materials," *Progress In Electromagnetics Research*, Vol. 142, 31–40, 2013.
7. Liu, X., C. Li, K. Yao, X. K. Meng, W. Feng, B. H. Wu, and F. Li, "Experimental verification of broadband invisibility using a cloak based on inductor-capacitor networks," *Applied Physics Letters*, Vol. 95, No. 19, 191107, 2009.
8. Rajput, A. and K. V. Srivastava, "Arbitrary shaped reciprocal external cloak with nonsingular and homogeneous material parameters using expanding coordinate transformation," *Plasmonics*, Vol. 12, No. 3, 771–781, 2017.

9. Li, C. Y., L. Xu, L. L. Zhu, S. Y. Zou, Q. H. Liu, Z. Y. Wang, and H. Y. Chen, "Concentrators for water waves," *Physical Review Letters*, Vol. 121, No. 10, 104501, 2018.
10. Yang, C. F., M. Huang, J. J. Yang, T. H. Li, F. C. Mao, and P. Li, "Arbitrarily shaped homogeneous concentrator and its layered realization," *Optics Communications*, Vol. 435, 150–158, 2019.
11. Madni, H. A., K. Hussain, W. X. Jiang, S. Liu, A. Aziz, A. Iqbal, A. Marhoob, and T. J. Cui, "A novel EM concentrator with open-concentrator region based on multi-folded transformation optics," *Scientific Reports*, Vol. 8, No. 1, 1–10, 2018.
12. Zang, X. F., J. J. Li, J. F. Mao, and C. Jiang, "Experimental demonstration of the wave squeezing effect based on inductor-capacitor networks," *Applied Physics Letters*, Vol. 101, No. 7, 074104, 2012.
13. Yang, C. F., M. Huang, J. J. Yang, F. C. Mao, and T. H. Li, "Target illusion by shifting a distance," *Optics Express*, Vol. 26, No. 19, 24280–24293, 2018.
14. Yi, J. J., P. H. Tichit, S. N. Burokur, and A. de Lustrac, "Illusion optics: Optically transforming the nature and the location of electromagnetic emissions," *Journal of Applied Physics*, Vol. 117, No. 8, 084903, 2015.
15. Yi, J. J., S. N. Burokur, and A. de Lustrac, "Experimental validation of a transformation optics-based lens for beam steering," *Applied Physics Letters*, Vol. 107, No. 15, 154101, 2015.
16. Ebrahimpouri, M. and O. Quevedo-Teruel, "Bespoke lenses based on quasi-conformal transformation optics technique," *IEEE Transactions on Antennas and Propagation*, Vol. 65, No. 5, 2256–2264, 2017.
17. Yuan, S. H., Y. Y. Zhang, Q. Y. Zhang, B. S. Zou, and U. Schwingenschogl, "Curvature effects in two-dimensional optical devices inspired by transformation optics," *Applied Physics Letters*, Vol. 109, No. 20, 201105, 2016.
18. Yi, J. J., M. T. Guo, R. Feng, B. Ratni, L. N. Zhu, D. H. Wenner, and S. N. Burokur, "Design and validation of an all-dielectric metamaterial medium for collimating orbital-angular-momentum vortex waves at microwave frequencies," *Physical Review Applied*, Vol. 12, No. 3, 034060, 2019.
19. Yang, Y., X. M. Zhao, and T. J. Wang, "Design of arbitrarily controlled multi-beam antennas via optical transformation," *Journal of Infrared, Millimeter, and Terahertz Waves*, Vol. 30, No. 4, 337, 2009.
20. Cheng, Q., W. Xiang, and T. J. Cui, "Multi-beam generations at pre-designed directions based on anisotropic zero-index metamaterials," *Applied Physics Letters*, Vol. 99, No. 13, 131913, 2011.
21. Wu, Q., Z. H. Jiang, O. Quevedo-Teruel, J. P. Turpin, W. X. Tang, Y. Hao, and D. H. Werner, "Transformation optics inspired multibeam lens antennas for broadband directive radiation," *IEEE Transactions on Antennas and Propagation*, Vol. 61, No. 12, 5910–5922, 2013.
22. Tichit, P. H., S. N. Burokur, and A. de Lustrac, "Spiral-like multi-beam emission via transformation electromagnetics," *Journal of Applied Physics*, Vol. 115, No. 2, 024901, 2014.
23. Zhang, K., X. M. Ding, D. L. Wo, F. R. Meng, and Q. Wu, "Experimental validation of ultra-thin metalenses for N-beam emissions based on transformation optics," *Applied Physics Letters*, Vol. 108, No. 5, 053508, 2016.
24. Zhu, C. H., Z. G. Jiang, L. J. Liu, N. Liu, and Q. H. Liu, "A new strategy for transformation optics with index-only media," *IEEE Transactions on Antennas and Propagation*, Vol. 67, No. 7, 4626–4635, 2019.
25. Caloz, C. and T. Itoh, *Electromagnetic Metamaterials: Transmission Line Theory and Microwave Applications*, John Wiley & Sons, 2005.
26. Li, C., X. K. Meng, X. Liu, F. Li, G. Y. Fang, H. Y. Chen, and C. T. Chan, "Experimental realization of a circuit-based broadband illusion-optics analogue," *Physical Review Letters*, Vol. 105, No. 23, 233906, 2010.
27. Zang, X. F., Y. M. Zhu, X. B. Ji, L. Chen, Q. Hu, and S. L. Zhuang, "Broadband unidirectional behavior of electromagnetic waves based on transformation optics," *Scientific Reports*, Vol. 7, 40941, 2017.